Hindawi
Shock and Vibration
Volume 2022, Article ID 5229481, 11 pages
https://doi.org/10.1155/2022/5229481

Research Article

Dynamic Investigation and Resonant Frequency Determination of Shaft Bending Fatigue Testing Machine

Jinghe Zhao, Ying Zhang, and Bo Jiang

School of Mechanical Engineering, Changchun Guanghua University, Changchun 130033, China

Correspondence should be addressed to Jinghe Zhao; zhaojinghe-1982@163.com

Received 6 April 2022; Revised 8 July 2022; Accepted 27 July 2022; Published 18 August 2022

Academic Editor: Francesco Bucchi

The testing machine of shaft bending fatigue is widely used to test the fatigue limit and life of various shaft-type parts in mechanical engineering. Machine dynamic characteristics and system bending resonant frequency are very important for the design, testing, and application of the testing machine, but existing complex finite element calculation and aimless large-range frequency scanning in testing are the available methods to solve these two problems helplessly and inefficiently. A novel analytical model of nonlinear coupling dynamic system is built for the fatigue testing machine in this paper. The nonlinear dynamic model is simulated and investigated numerically, then it is reasonably linearized and reduced as a linear one, and the corresponding error analysis and application range are presented. By using eigenvalue approximation, the shaft bending resonant frequency formula is obtained, then the formula is compared and verified with the results from the nonlinear system simulation and finite element software, and it can improve the machine design and testing efficiency obviously. The analytical dynamic modeling and linearizing, and the given mode resonant frequency approximating, also provide a reference for many similar vibration machines.

1. Introduction

Shaft-type parts are widely used to transmit motion and power in mechanical systems. However, most shaft part failure results from fatigue damage. The shaft is generally subjected to bending action in service, and its bending fatigue resistance is a key concern in design and application. As indicated by Mohammadi et al. [1], improving bending fatigue strength of a mechanical part and reducing its weight meet the requirement of lightweight constructional design. The bending fatigue test is very essential to bending fatigue performance of shaft parts from Carpinteri and Spagnoli[2] and Schmid et al. [3]. Especially, for the shafts with complex shapes, such as the crankshaft of an internal combustion engine, the bending fatigue test becomes an indispensable process in design and manufacture, due to the difficulty in quantifying the complex shape and impact of various strengthening processes practically and accurately in Yu et al. [4].

Shaft resonant bending fatigue test is one of the most common and efficient testing ways for the shaft fatigue limit and life assessments. According to the principle of structural resonance in Huertas et al. [5], the exciting frequency should be near the resonant frequency of the fatigue testing system to just cause the bending resonance of the shaft parts, and then the tested shaft can be subjected to the largest bending load. Many researchers have focused on the theory and experiment of the bending fatigue test. Mohammadi et al. [1] predicted the fatigue life of a notched shaft under bending load. Huertas et al. [5] designed, fabricated, and assessed a resonant plate test bench for shaft fatigue testing to reduce testing time. Yu et al. [6] researched on the impact of notch depth on the resonant frequency of the system with notched crankshaft sections. Zhou and Yu [7] obtained the fatigue crack propagation characteristics of a crankshaft by the frequency sweep method. Lü et al. [8] studied free and forced bending vibrations of a crankshaft by a distributed continuous model. Kasprzyczak and Macha [9] introduced an electromechanical fatigue stand for polyharmonic bending and torsion, and its strain energy parameter control algorithm. Bao et al. [10] calculated residual stress and bending stress of fillet rolled crankshaft by the finite element method.

Spiteri and Segar[11] monitored resonance shifts of tested crankshafts and found that accelerating resonance shift was a signal of failure. DCX Stress Lab and Tool Development & Test Support groups developed an efficient automatic computerized digital resonance fatigue testing system. Dongfeng Motor Co., Ltd. [12] developed a computerized electrodynamic resonant fatigue test machine, which is used for bending, torsional, and bending-torsional complex fatigue tests of crankshaft in Feng [13].

However, until now, few works have been done on a systematic investigation of machine dynamic characteristics and an analytical determination of the resonant frequency for the shaft bending fatigue testing system.

In this paper, a shaft fatigue testing machine is illustrated and modeled as an 8-degree of freedom (DOF) nonlinear coupling dynamic system. By solving the nonlinear coupling dynamic equations numerically, the shaft fatigue testing system is simulated and analyzed under different shaker exciting frequencies and amplitudes. The nonlinear dynamic model is reduced and linearized, and the corresponding error analysis and application range are carried out and presented. An analytical shaft bending resonant frequency is obtained in a formula, which is very convenient for practical application and agrees with the finite element software results very well.

2. System Modeling

Similar to the machine structure in References [5, 6, 10–13], a testing machine of shaft bending fatigue is designed and illustrated in Figure 1. A tested shaft is fixed at its two ends to two pendulum blocks (plates or tines), and each pendulum block is connected to the suspending system (including the frame, roller, and its bed) by flexible wireropes. The suspending rollers, flexible wireropes, and pendulum blocks can move freely along the roller beds horizontally. The suspending frame can be lifted vertically by the elevating system of wirerope and pulley, and even be fixed by the locking mechanism. The right pendulum block is excited by an electromagnetic shaker as a harmonic exciting force at an assigned frequency and amplitude.

A simplified in-plane structural dynamic model of the shaft bending fatigue testing machine is illustrated in Figure 2. The left/right pendulum block is simplified as a rigid body with lumped mass m and rotational inertia I with respect to the centroids C_1 and C_2. For each pendulum block, the suspending wireropes are simplified as a spring with an initial length L and lumped stretching stiffness k, whereas their mass is very small and negligible. The hinge point between a suspending wirerope end and a pendulum block is P_1 and P_2. The suspending roller is simplified as a ring with mass m_0 which can move freely along a horizontal rigid beam modeled from the roller bed. The right pendulum block is excited by the electromagnetic shaker in a way of harmonic force $F = A_F \sin(\omega t)$ at point Q, and the vertical distance from the pendulum block centroid to point Q is D. The fixing points between a tested shaft and the pendulum block are Q_1 and Q_2. The vertical distance from the pendulum block centroid to the shaft axis is G, and that to the wirerope end is H. The pendulum block width is $2W$, and the horizontal distance from shaft end $Q_{1,2}$ to wirerope end $P_{1,2}$ is B. Compared with the left and right large rigid pendulum blocks, the mass of tested shaft is so small that it can be neglected.

In addition, the tested shaft is simplified as three equivalent in-plane springs, respectively, a force bending spring with stiffness K_F, a moment bending spring with stiffness K_M, and an axial normal spring with stiffness K_N, and with the shaft two fixing ends Q_1 and Q_2. These three stiffnesses can be determined by analytical formulas for regular shape shafts, or by finite element numerical calculations for complex shape shafts, or even by some experimental measurement results.

In the running process of the shaft bending fatigue testing machine, some translational and angular displacements appear due to system vibration coupling effects: the horizontal displacements of suspending roller rings are assumed as X_1 and X_2, the suspending wirerope total elongations are assumed as s_1 and s_2, the swing angles of wirerope are assumed as α_1 and α_2, and the swing angles of pendulum blocks are assumed as β_1 and β_2. The horizontal displacements of the left and right pendulum blocks are assumed as x_1 and x_2, and the vertical ones are assumed as y_1 and y_2, as defined in Figure 2(b).

In Figure 2(b) for the system vibrating status of the shaft bending fatigue testing machine, the coordinates of points $P_{1,2}$, $Q_{1,2}$, and Q can be expressed as follows:

$$x_{P1} = X_1 - (L + s_1)\sin(\alpha_1) = x_1 + H \sin(\beta_1), \quad (1)$$

$$y_{P1} = (L + s_1)\cos(\alpha_1) = y_1 - H \cos(\beta_1), \quad (2)$$

$$x_{P2} = X_2 - (L + s_2)\sin(\alpha_2) = x_2 + H \sin(\beta_2), \quad (3)$$

$$y_{P2} = (L + s_2)\cos(\alpha_2) = y_2 - H \cos(\beta_2), \quad (4)$$

$$x_{Q1} = x_1 + G \sin(\beta_1) + B \cos(\beta_1), \quad (5)$$

$$y_{Q1} = y_1 - G \cos(\beta_1) + B \sin(\beta_1), \quad (6)$$

$$x_{Q2} = x_2 + G \sin(\beta_2) - B \cos(\beta_2), \quad (7)$$

$$y_{Q2} = y_2 - G \cos(\beta_2) - B \sin(\beta_2), \quad (8)$$

$$x_Q = x_2 - D \sin(\beta_2) + W \cos(\beta_2), \quad (9)$$

$$y_Q = y_2 + D \cos(\beta_2) + W \sin(\beta_2). \quad (10)$$

In addition, some translational and angular displacements in Figure 2 can be related with others due to system inherent geometric relationships,

$$s_1 = \frac{y_1 - H \cos \beta_1}{\cos \alpha_1} - L, \quad (11)$$

$$s_2 = \frac{y_2 - H \cos \beta_2}{\cos \alpha_2} - L, \quad (12)$$

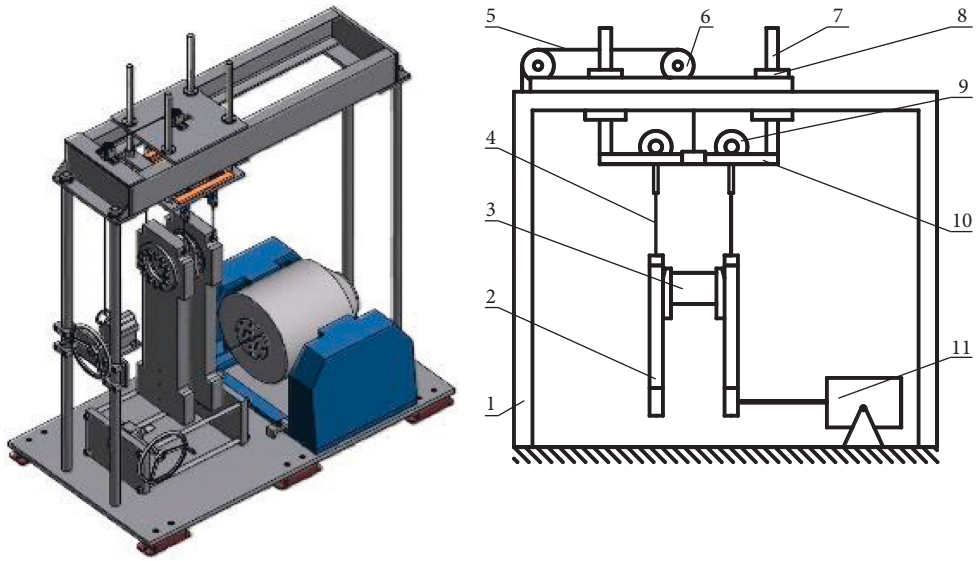

Figure 1: A testing machine of shaft bending fatigue. (a) Three-dimensional presentation, (b) two-dimensional schematic diagram. In (b), 1: machine rack, 2: pendulum block, 3: tested shaft, 4: suspending wirerope, 5: elevating wirerope, 6: elevating pulley, 7: suspending frame, 8: locking mechanism, 9: suspending roller, 10: suspending roller bed, 11: electromagnetic shaker.

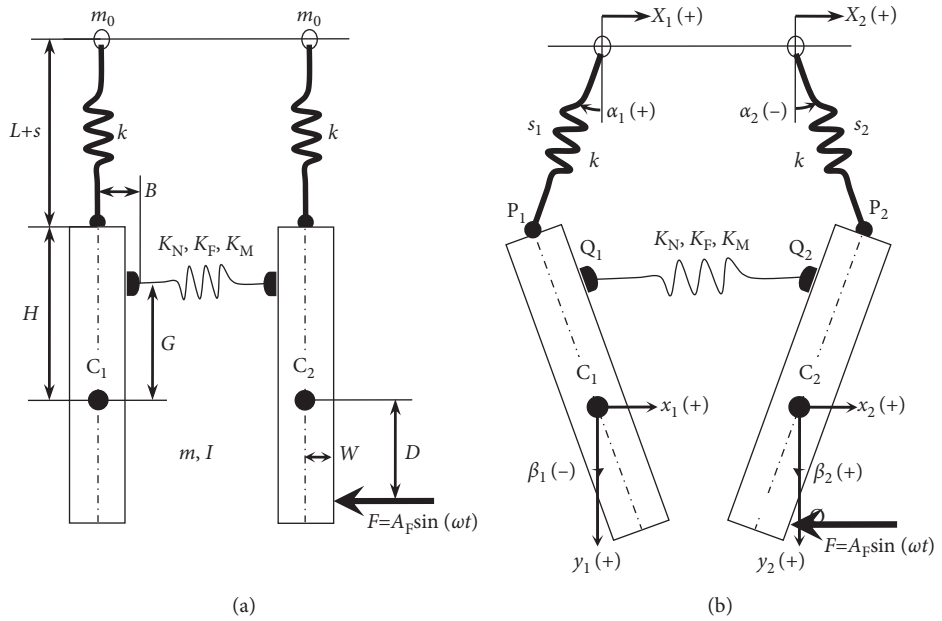

Figure 2: A simplified in-plane model of the shaft bending fatigue testing machine. (a) Equilibrium status, (b) vibrating status.

$$\alpha_1 = \arctan\frac{x_1 - X_1 + H\sin\beta_1}{H\cos\beta_1 - y_1}, \tag{13}$$

$$\alpha_2 = \arctan\frac{x_2 - X_2 + H\sin\beta_2}{H\cos\beta_2 - y_2}. \tag{14}$$

With Newton's second law, the horizontal translational motions X_1 and X_2 with damping of the left and right rings with mass m_0 can be governed as (15) and (16) under the action of suspending wirerope; the horizontal and vertical displacements $x_{1,2}$ and $y_{1,2}$ with damping of left and right pendulum block centroid with mass m can be formulated as (17)–(20), respectively, under the action of gravity, suspending wirerope, shaft equivalent forces, and shaker exciting force; the swing angles $\beta_{1,2}$ around the centroid point $C_{1,2}$ of left and right pendulum blocks with rotational inertia I can be governed as (21) and (22) with damping under the

action of suspending wirerope, shaft equivalent forces, and shaker exciting moment.

$$m_0\ddot{X}_1 = -\eta_{X1}\dot{X}_1 - ks_1 \sin(\alpha_1), \tag{15}$$

$$m_0\ddot{X}_2 = -\eta_{X2}\dot{X}_2 - ks_2 \sin(\alpha_2), \tag{16}$$

$$m\ddot{x}_1 = -\eta_{x1}\dot{x}_1 + ks_1 \sin(\alpha_1) + K_N\left(x_{Q2} - x_{Q1} + 2B\right), \tag{17}$$

$$m\ddot{y}_1 = -\eta_{y1}\dot{y}_1 - ks_1 \cos(\alpha_1) + K_F\left(y_{Q2} - y_{Q1}\right) + mg, \tag{18}$$

$$\begin{aligned} m\ddot{x}_2 = {} & -\eta_{x2}\dot{x}_2 + 2ks_2 \sin(\alpha_2) \\ & + K_N\left(x_{Q1} - x_{Q2} - 2B\right) - F, \end{aligned} \tag{19}$$

$$m\ddot{y}_2 = -\eta_{y2}\dot{y}_2 - ks_2 \cos(\alpha_2) + K_F\left(y_{Q1} - y_{Q2}\right) + mg, \tag{20}$$

$$\begin{aligned} I\ddot{\beta}_1 = {} & -\eta_{\beta1}\dot{\beta}_1 + ks_1 H \sin(\alpha_1 - \beta_1) + K_M(\beta_2 - \beta_1) \\ & + K_N\left(x_{Q2} - x_{Q1} + 2B\right)G \cos(\beta_1) \\ & + K_F\left(y_{Q2} - y_{Q1}\right)B \cos(\beta_1), \end{aligned} \tag{21}$$

$$\begin{aligned} I\ddot{\beta}_2 = {} & -\eta_{\beta2}\dot{\beta}_2 + ks_2 H \sin(\alpha_2 - \beta_2) + K_M(\beta_1 - \beta_2) \\ & + K_N\left(x_{Q1} - x_{Q2} - 2B\right)G \cos(\beta_2) \\ & + K_F\left(y_{Q1} - y_{Q2}\right)B \cos(\beta_2) + F\ D \cos(\beta_2), \end{aligned} \tag{22}$$

where the shaker exciting force is written as $F = A_F\sin(\omega t)$ in the way of harmonic fluctuating; the terms $\eta_{X1,2}$, $\eta_{x1,2}$, $\eta_{y1,2}$, and $\eta_{\beta1,2}$ are the proportional damping parameters for each displacement vibration. As a result, an 8-DOF nonlinear coupling dynamic equation system of the shaft bending fatigue testing machine is modeled with respect to eight independent translational and angular displacements ($X_{1,2}$, $x_{1,2}$, $y_{1,2}$, $\beta_{1,2}$).

In the equilibrium case of pendulum blocks without swing angles $\beta_{1,2} = 0$ and displacements $x_{1,2} = 0$, the horizontal distance between the shaft two fixing ends Q_1 and Q_2 is the free length L_d of tested shaft. Under the pendulum block swing angles $\beta_{1,2}$ and displacements $x_{1,2}$, and with respect to the equilibrium positions of the left and right pendulum block centroid point $C_{1,2}$, the horizontal positions $x_{Q1,2}$ at the shaft two fixing ends Q_1 and Q_2 points are written as (5) and (7). Then the horizontal distance between Q_1 and Q_2 becomes $(B + L_d + B + x_{Q2})$-x_{Q1}, where $B + L_d + B$ is the fundamental structural distance between the left and right centroid point $C_{1,2}$. As a result, the distance difference can be written as $\Delta_N = [(B + L_d + B + x_{Q2}) - x_{Q1}] - L_d = x_{Q2} - x_{Q1} + 2B$. Finally, the axial normal load acting on the tested shaft can be determined as $F_N = K_N\Delta_N = K_N(x_{Q2} - x_{Q1} + 2B)$.

Similarly, the force bending load can be determined as $F_B = K_F(y_{Q2} - y_{Q1})$, and the moment bending load can be determined as $M_B = K_M(\beta_2 - \beta_1)$.

3. Nonlinear Simulation

The dynamic (15)–(22) are highly nonlinearly coupled, and it is very hard to obtain an analytical solution. In this paper, the dynamic equation system is solved by using the numerical Runge–Kutta method to obtain an instantaneous response of the independent translational and angular displacements ($X_{1,2}$, $x_{1,2}$, $y_{1,2}$, $\beta_{1,2}$).

For a real shaft bending fatigue testing machine, the system structural inherent parameters are listed in Table 1 for the following numerical simulation and analysis. Without loss of generality, a crankshaft is selected as a tested shaft sample for a common dynamic characteristics' investigation, and above equivalent shaft stiffnesses can be determined as $K_N = 3.1008 \times 10^9$ N/m, $K_F = 2.3256 \times 10^7$ N/m, and $K_M = 1.7124 \times 10^6$ N•m/rad by using the finite element calculation.

The instantaneous response history of the translational and angular displacements ($X_{1,2}$, $s_{1,2}$, $x_{1,2}$, $y_{1,2}$, $\alpha_{1,2}$, and $\beta_{1,2}$) and the loads (F_N, F_B and M_B) acting on the tested shaft are illustrated in Figure 3 at the exciting frequency $\omega = 30$ Hz and amplitude $A_F = 5$ kN in the view of engineering practice of general shaft bending fatigue testing machine and references Huertas et al. [5] and Zhou and Yu [7]. Under the harmonic exciting force $F = A_F\sin(\omega t)$, all responses go through from initial instantaneous step to steady-state harmonically fluctuating step just with the frequency ω. In practice, the testing machine is always running at the steady-state harmonically fluctuating step, and the harmonically reciprocating fatigue loads (F_N, F_B, M_B) are induced and acted on the tested shaft. The tested shaft fatigue loads are caused by the relative motions of the translational and angular displacements ($x_{Q1,2}$, $y_{Q1,2}$, $\beta_{1,2}$), respectively, and a large-amplitude opposite motion can result in a large-amplitude fatigue load correspondingly. As a result, a proper exciting frequency ω should cause the tested shaft bending resonance with symmetrically large-amplitude opposite angular displacements β_1 and β_2, and then a large-amplitude bending fatigue moment load M_B can be obtained in the tested shaft.

With respect to different values of exciting frequency ω and amplitude A_F of shaker force F, the amplitude of the roller ring related to translational displacement $X_r = X_2 - X_1$ and the loads (F_N, F_B, M_B) acting on the tested shaft are illustrated in Figure 4, since the amplitude of the tested shaft loads is a crucial performance indicator for the shaft bending fatigue testing machine. As shown in Figure 4, the amplitudes of X_r and F_B are larger, in general, at a lower exciting frequency ω and a larger exciting force amplitude A_F, but they increase somewhat when the exciting frequency ω approaches 38.5 Hz. In addition, the local maximum amplitude of F_B takes place at the exciting frequency ω near 125.5 Hz. The universal maximum amplitudes of F_N and M_B appear at the exciting frequency ω near 38.5 Hz, and they increase with the increase of A_F at this exciting frequency. Therefore, the shaft bending resonance frequency in the testing system can be recognized as 38.5 Hz.

Table 1: Structural inherent parameters of the testing machine.

Parameters	B (m)	H (m)	G (m)	D (m)	m_0 (kg)	k (N/m)	m (kg)	I (kg•m^2)
Values	0.035	0.670	0.470	0.365	2.20	6×10^7	171.5	20.54

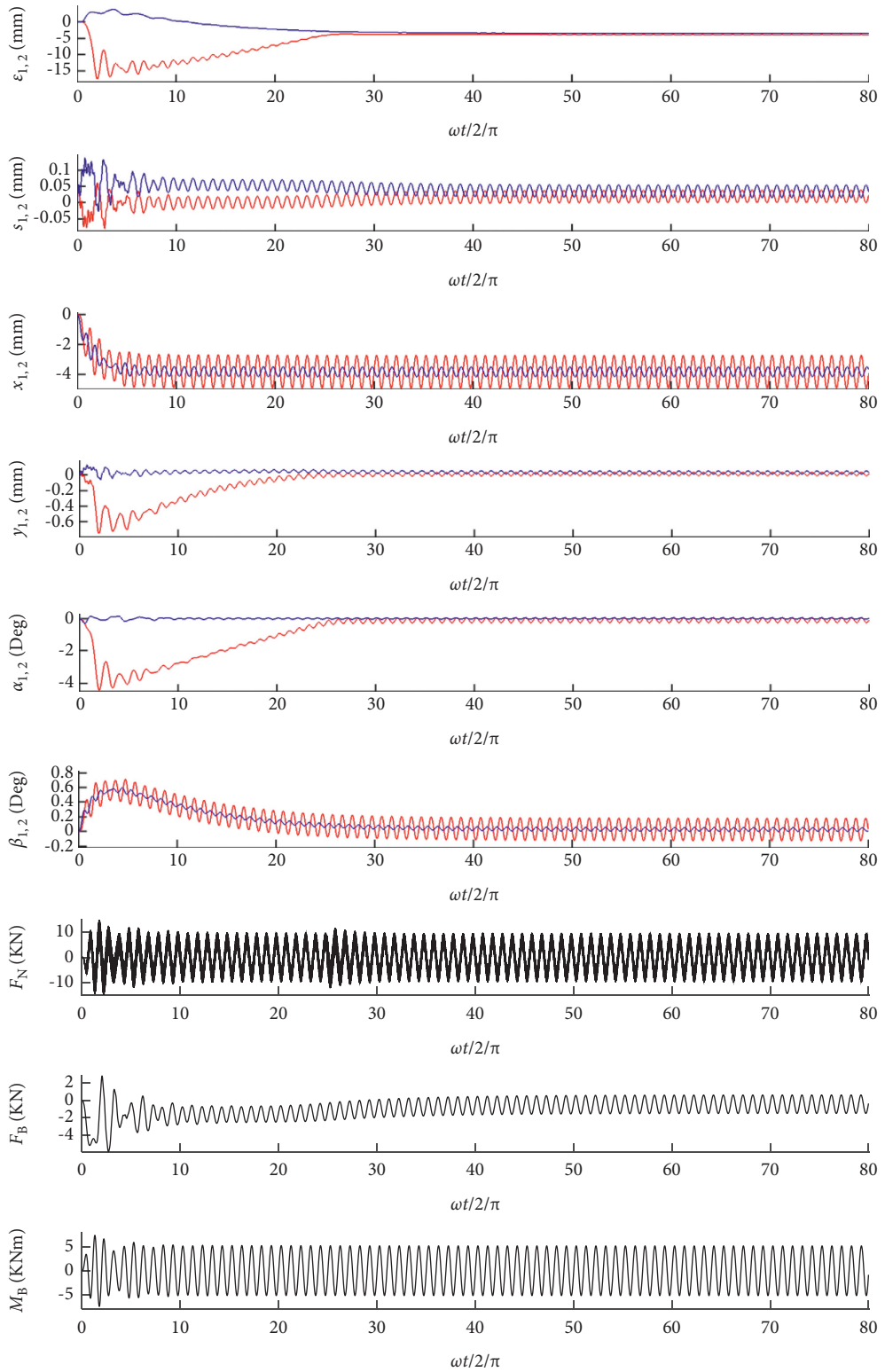

Figure 3: Instantaneous response history of the translational and angular displacements and the tested shaft loads. Numerical solution at $\omega = 30$ Hz and $A_F = 5$ kN. Red line: (X_1, s_1, x_1, y_1, α_1, β_1), blue line: (X_2, s_2, x_2, y_2, α_2, β_2).

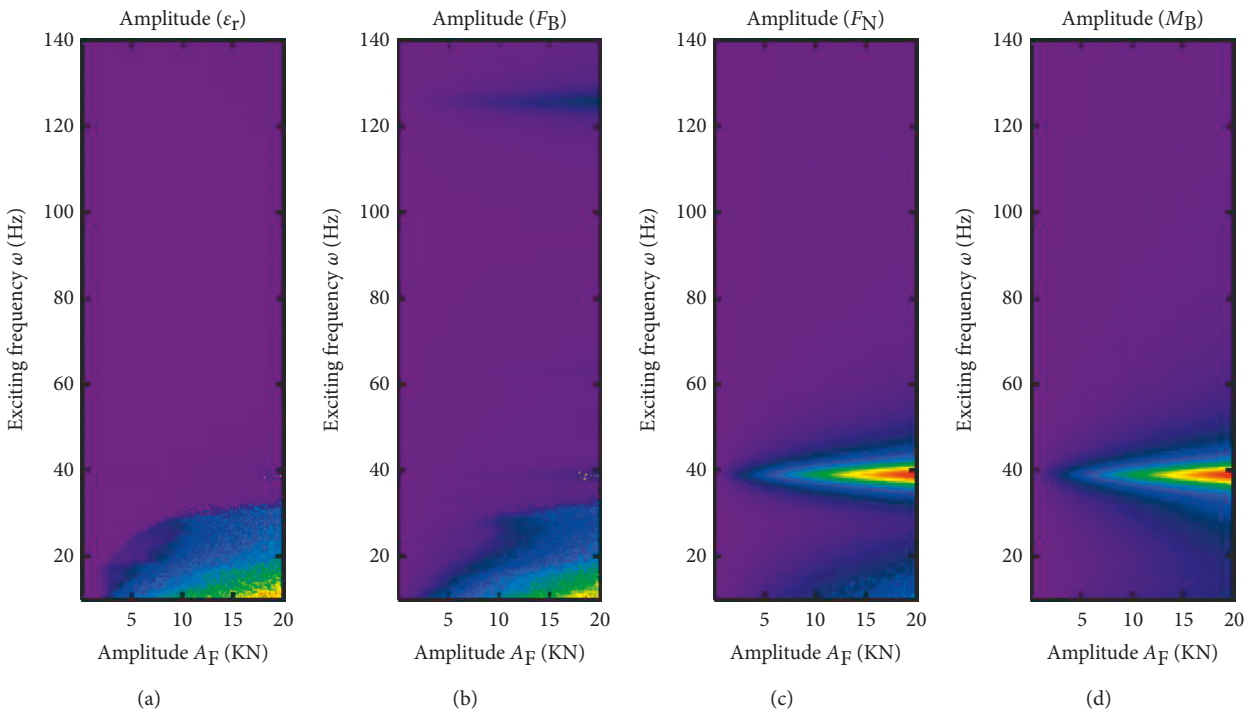

Figure 4: Amplitude of the roller ring relative displacement and the tested shaft loads with respect to the shaker exciting frequency and amplitude.

4. System Linearization

In the generally practical case of the shaft bending fatigue testing machine, the amplitude of the shaker acting at the pendulum block (in meter) is always as small as several millimeters, then the swing angles $\alpha_{1,2}$ and $\beta_{1,2}$ are small value items. As a common linearization approximation process, it can be approximated that $\sin(\alpha_{1,2}) \approx \alpha_{1,2}$, $\sin(\beta_{1,2}) \approx \beta_{1,2}$, $\cos(\alpha_{1,2}) \approx 1$, and $\cos(\beta_{1,2}) \approx 1$ mathematically. In addition, the suspending wirerope elongation can be separated in two parts: a larger gravity deformation and a very small vibrational elongation, thus $s_1 = \mathrm{mg/k} + z_1$ and $s_2 = \mathrm{mg/k} + z_2$ are introduced to simplify calculation by the wirerope small vibrational elongation $z_{1,2}$. In (15) and (16), one has $ks_{1,2}\sin(\alpha_{1,2}) = mg\sin(\alpha_{1,2}) + kz_{1,2}\sin(\alpha_{1,2})$, where $\alpha_{1,2}$ and $z_{1,2}$ are small items, then the first-order linearization form can be expressed as $ks_{1,2}\sin(\alpha_{1,2}) \approx \mathrm{mg}\alpha_{1,2}$ for (23) and (24). Similarly, after the same operations of substituting the small items (z_1, z_2, α_1, α_2, β_1, β_2) in (1)–(14) and (17)–(22), just retaining first-order linearization form, and neglecting high order terms, then the undamped nonlinear dynamic system ((15)–(22)) can be reduced and linearized as

$$m_0\ddot{X}_1 + mg\alpha_1 = 0, \tag{23}$$

$$m_0\ddot{X}_2 + mg\alpha_2 = 0, \tag{24}$$

$$m\ddot{z}_1 + kz_1 + K_F B(\beta_1 + \beta_2) + K_F(z_1 - z_2) = 0, \tag{25}$$

$$m\ddot{z}_2 + kz_2 - K_F B(\beta_1 + \beta_2) + K_F(z_2 - z_1) = 0, \tag{26}$$

$$mL_s\ddot{\alpha}_1 + mH\ddot{\beta}_1 - m\ddot{X}_1 + K_N L_s(\alpha_1 - \alpha_2) + K_N(H - G)(\beta_1 - \beta_2) + mg\alpha_1 + K_N(X_1 - X_2) = 0, \tag{27}$$

$$mL_s\ddot{\alpha}_2 + mH\ddot{\beta}_2 - m\ddot{X}_2 + K_N L_s(\alpha_2 - \alpha_1) + K_N(H - G)(\beta_2 - \beta_1) + mg\alpha_2 + K_N(X_1 - X_2) = F, \tag{28}$$

$$I\ddot{\beta}_1 + mgH(\beta_1 - \alpha_1) + K_N L_s G(\alpha_2 - \alpha_1) + K_{NM}(\beta_2 - \beta_1) + K_F B^2(\beta_1 + \beta_2) + K_N G(X_1 - X_2) = 0, \tag{29}$$

$$I\ddot{\beta}_2 + mgH(\beta_2 - \alpha_2) + K_N L_s G(\alpha_1 - \alpha_2) + K_{NM}(\beta_1 - \beta_2) - K_F B^2(\beta_1 + \beta_2) + K_N G(X_2 - X_1) = F\ D, \tag{30}$$

where $K_{\mathrm{NM}} = K_N G(H - G) - K_M$, and $L_s = L + \mathrm{mg/k}$; the proportional damping terms $\eta_{X1,2}$, $\eta_{x1,2}$, $\eta_{y1,2}$, and $\eta_{\beta 1,2}$ are all neglected for the numerical convenience of the following analytical discussion on system natural frequency.

The linearized undamped dynamic system ((23)–(30)) can be collected in matrix form as follows:

$$\mathbf{M}\ddot{\mathbf{x}} + \mathbf{K}\mathbf{x} = F\mathbf{f}, \tag{31}$$

where $x = [X_1, X_2, z_1, z_2, \alpha_1, \alpha_2, \beta_1, \beta_2]^{\mathrm{T}}$, $f = [0, 0, 0, 0, 0, 0, 1, 0, \mathrm{D}]^{\mathrm{T}}$;

$$\mathrm{M} = \begin{bmatrix} m_0 & 0 & 0 & 0 & 0 & 0 & 0 & 0 \\ 0 & m_0 & 0 & 0 & 0 & 0 & 0 & 0 \\ 0 & 0 & m & 0 & 0 & 0 & 0 & 0 \\ 0 & 0 & 0 & m & 0 & 0 & 0 & 0 \\ -m & 0 & 0 & 0 & mL_s & 0 & mH & 0 \\ 0 & -m & 0 & 0 & 0 & mL_s & 0 & mH \\ 0 & 0 & 0 & 0 & 0 & 0 & I & 0 \\ 0 & 0 & 0 & 0 & 0 & 0 & 0 & I \end{bmatrix}, \quad (32)$$

$$\mathbf{K_1} = \begin{bmatrix} 0 & 0 & 0 & 0 \\ 0 & 0 & 0 & 0 \\ 0 & 0 & k + K_\mathrm{F} & -K_\mathrm{F} \\ 0 & 0 & -K_\mathrm{F} & k + K_\mathrm{F} \\ -K_\mathrm{N} & K_\mathrm{N} & 0 & 0 \\ K_\mathrm{N} & -K_\mathrm{N} & 0 & 0 \\ K_\mathrm{N}G & -K_\mathrm{N}G & 0 & 0 \\ -K_\mathrm{N}G & K_\mathrm{N}G & 0 & 0 \end{bmatrix}, \text{ and}$$

$$\mathbf{K_2} = \begin{bmatrix} mg & 0 & 0 & 0 \\ 0 & mg & 0 & 0 \\ 0 & 0 & K_\mathrm{F}B & K_\mathrm{F}B \\ 0 & 0 & -K_\mathrm{F}B & -K_\mathrm{F}B \\ mg + K_\mathrm{N}L_s & -K_\mathrm{N}L_s & K_\mathrm{N}(H-G) & -K_\mathrm{N}(H-G) \\ -K_\mathrm{N}L_s & mg + K_\mathrm{N}L_s & -K_\mathrm{N}(H-G) & K_\mathrm{N}(H-G) \\ -mgH - K_\mathrm{N}L_sG & K_\mathrm{N}L_sG & mgH - K_\mathrm{NM} + K_\mathrm{F}B^2 & K_\mathrm{NM} + K_\mathrm{F}B^2 \\ K_\mathrm{N}L_sG & -mgH - K_\mathrm{N}L_sG & K_\mathrm{NM} - K_\mathrm{F}B^2 & mgH - K_\mathrm{NM} - K_\mathrm{F}B^2 \end{bmatrix}. \quad (33)$$

The stiffness matrix K is deduced originally from the solid physical nonlinear dynamic system (15)–(22) with sophisticated mechanic modeling, then some common approximation and linearization are used mathematically with some small value items and neglecting high order terms in the formula. In the stiffness matrix K mathematical deduction, the approximation and linearization may be a reason to result in its asymmetry. In addition, different from the common dynamic system with complete constraints and boundary conditions with a symmetrical stiffness matrix, the structure of shaft bending fatigue testing machine is a special problem as shown in Figures 1 and 2, it can have free motion freedom $X_{1,2}$ at least, and even the common constraints and boundary conditions cannot be found. This may be another reason to result in the unsymmetrical stiffness matrix K.

5. Resonant Frequency

As indicated in Figure 4, a quite exciting frequency should be selected and generated by the shaker in the view of energy conservation and efficiency improvement, and the right exciting frequency can just cause the shaft part bending resonance in the testing machine.

For the linearized undamped dynamic system (31), system natural frequency ω_r and mode shape vector z can be determined by an eigenvalue problem,

$$\left(\mathbf{K} - \omega_r^2\mathbf{M}\right)z = 0. \quad (34)$$

Without any analytical deduction, derivation, and numerical assumption, but just using the solved eigenvector in (32) and the geometric relations in (1)–(14), the mode shape 1st to 8th is solved in Figure 5. In Figures 5(e) and 5(h), the shaft bending resonance takes place with symmetrically large opposite angular displacements β_1 and β_2, and the case in Figure 5(e) is more efficient and effective than that in Figure 5(h) because of a relatively larger swing angle $\beta_{1,2}$ of pendulum block, i.e. $\beta_{1,2} > \alpha_{1,2}$. An animation of system vibration mode shape 1st to 8th is made and attached in Video 1.

In the view of solution comparison and verification, a three-dimensional model of the main parts of the shaft bending fatigue testing machine is built and analyzed by the finite element commercial software ANSYS. In the ANSYS calculation, the top suspending roller bed is set as a rigid plate without deformation, the tetrahedral element is applied to the suspending wirerope, and the hexahedral element is applied to the tested shaft and pendulum block systems. In addition, the tested shaft and the pendulum block systems are modeled as a whole, since the tested shaft is fixed and clamped very solidly to the pendulum blocks in practice.

Convergence of the finite element result is studied in the view of the element size in Table 2. With the same element types presented in this table, the bending natural frequency as the machine working mode is used to indicate the finite element convergence with the element size selection in ANSYS. In addition, a more fine element size is selected around the connection between the suspending wirerope and pendulum block. As listed in Table 2, the calculation is convergent with the decrease of element size, and then the 10 mm element size is used as the final selection in the view of calculation accuracy and time consumption.

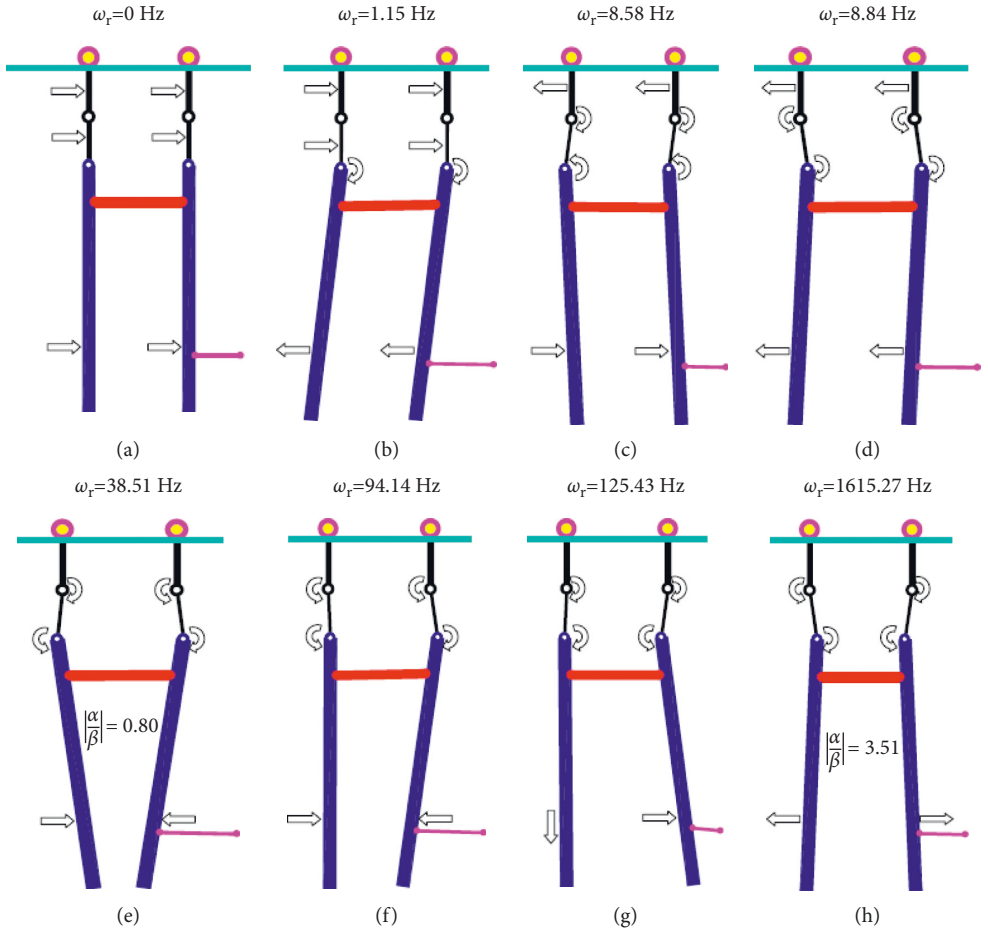

Figure 5: Natural frequency and mode shape results from the in-plane linearized model. (a) Mode 1st, (b) mode 2nd, (c) mode 3rd, (d) mode 4th, (e) mode 5th, (f) mode 6th, (g) mode 7th, and (h) mode 8th.

Table 2: Convergence of bending natural frequency with element size selection.

Element size (mm)	20	18	16	14	12	**10**
Frequency (Hz)	37.509	38.950	38.326	38.758	38.501	**38.601**

The natural frequency and mode shape results from a linear finite element analysis are illustrated in Figure 6, where the freely moving roller rings are neglected, and the suspending wireropes are connected to a fixed plate due to the limit of finite element available boundary condition.

As shown in Figures 5 and 6, the mode shape in Figure 5(c) with the natural frequency 8.58 Hz is identical to that in Figure 6(c) with the natural frequency 8.0022 Hz; the mode shape in Figure 5(e) with the natural frequency 38.51 Hz is identical to that in Figure 6(g) with the natural frequency 38.601 Hz, and that in Figure 4(c) with the natural frequency 38.5 Hz. However, other mode shapes in Figure 5 cannot be related to those given in Figure 6 directly, since the assumptions of structural in-plane motion, freely moving roller ring, rigid pendulum blocks, and lumped spring simplification of tested shaft are selected in this paper.

An analytical shaft bending resonant frequency given through a formula would be very convenient for practical application. As observed in Figures 3, 4(d), and 5(e) and the attached mode shape animation audio video interleaved (AVI), just for the shaft bending vibration mode, the translational displacements $X_{1,2}$ and $z_{1,2}$ are so small that they can be neglected, i.e. $X_{1,2} = z_{1,2} = 0$. The swing angles of the suspending wirerope and the pendulum block are almost symmetric, i.e. $\alpha_1 \approx -\alpha_2$ and $\beta_1 \approx -\beta_2$. The suspending wirerope and the pendulum block almost swing around the shaft clamping ends $Q_{1,2}$ proportionally, i.e. $L\alpha_{1,2} \approx -(H-G)\beta_{1,2}$; By comparing with the wirerope initial length L, the pendulum block's gravitational displacement mg/k and related terms are also so small and can be neglected. Finally, substituting above assumptions and small term reductions into the eigenvalue problem (32), using the symbolic calculation functions in Matlab software, and finding the eigenvalue and eigenvector just with respect to the shaft bending vibration mode, an analytical bending resonance frequency ω_n can then be obtained as

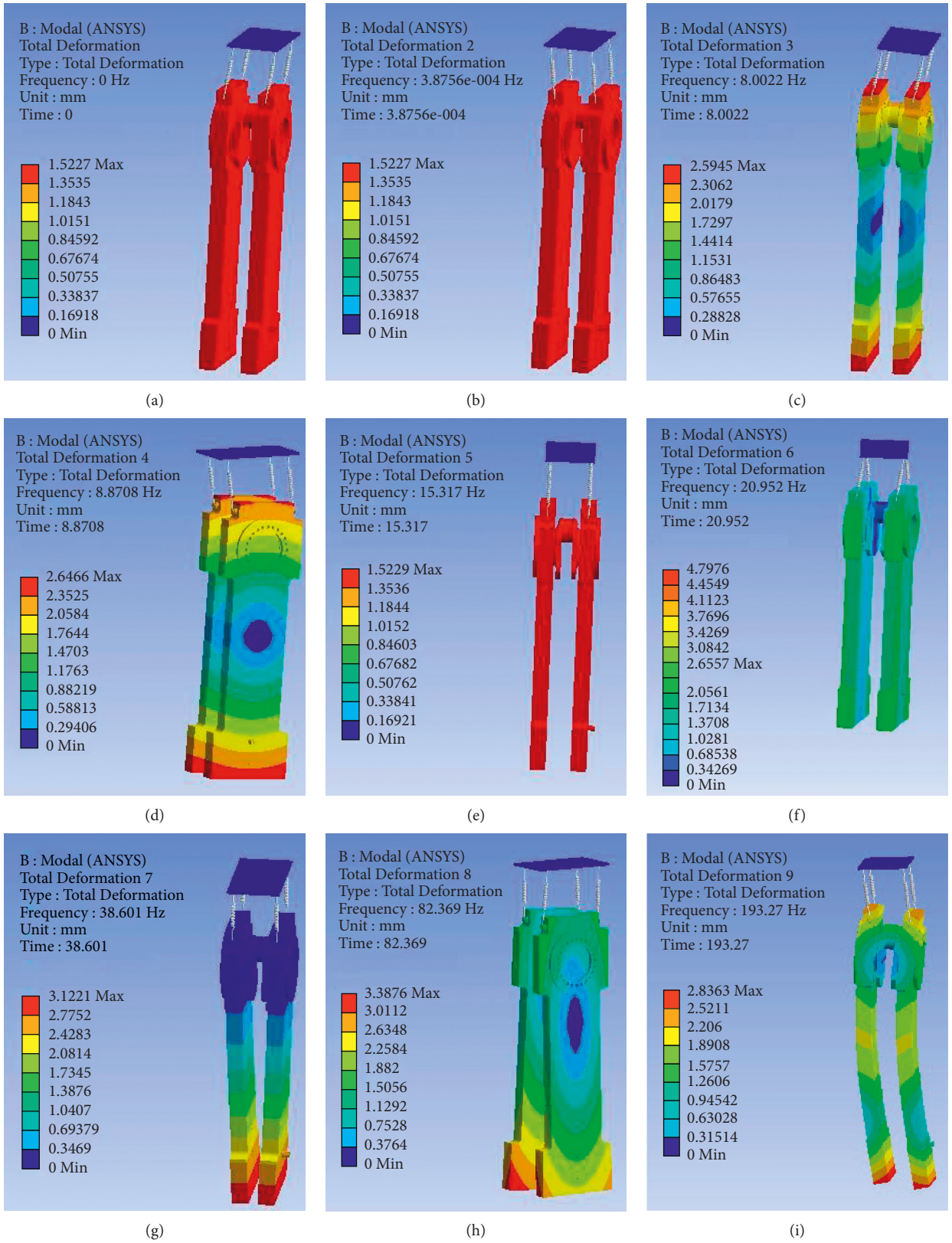

Figure 6: Natural frequency and mode shape results from the three-dimensional finite element model. (a) Mode 1st, (b) Mode 2nd, (c) mode 3rd, (d) mode 4th, (e) mode 5th, (f) mode 6th, (g) mode 7th, (h) mode 8th, and (i) mode 9th.

$$\omega_n = \sqrt{\frac{2\left(K_N/m\right)\left(K_M/I\right)}{\left(K_N/m\right)+\left(K_N G^2/I\right)+\left(K_M/I\right)}}. \quad (35)$$

With current machine parameters in this paper, the bending resonance frequency ω_n is predicted as 38.49 Hz from (33). Compared with the resonance frequency 38.51 Hz from the in-plane linearized undamped model in Figure 5(e), or that 38.601 Hz from the finite element undamped model in Figure 6(g), or that about 38.5 Hz from the in-plane nonlinear coupling damped model in Figure 4(c), the predicted resonance frequency ωn from the analytical formula ((33)) is acceptable.

As indicated in above assumptions from the nonlinear dynamic system (15)–(22) to the linearized one (23)–(30), the bending resonance frequency ω_n in (33) would be accurate just at small swing angles $\alpha_{1,2}$ and $\beta_{1,2}$, that is to say, the exciting amplitude A_F of shaker force should be small. However, as shown in Figure 4(c), the prediction of bending resonance frequency ω_n is acceptable even at the force exciting amplitude A_F as big as 20 kN ≈ 2 ton force; however, Huertas et al. [5] are with the maximum 10 kN, Zhou and Yu [7] is with 4318 Nm (about 4318/0.8 ≈ 5.4 KN). Even at the 20 kN force that is commonly out of range of an electromagnetic shaker's maximum output in the testing machine practice, effects of system nonlinearity on the natural frequency are not obvious as shown in Figure 4(c), and the prediction error of bending resonant frequency ω_n is not big and acceptable in practice.

6. Conclusions

In this paper, the testing machine of shaft bending fatigue is modeled as an eight degree-of-freedom (DOF) nonlinear coupling dynamic system with in-plane structures. Numerical simulation of the nonlinear system is carried out, the response history of system translational and angular displacements is analyzed, and the resonant frequency and corresponding vibration mode shape are observed and studied. Under the practical condition of small swing angular displacements, the nonlinear system is reasonably reduced as an in-plane linearized one. By comparing with the results from nonlinear system simulation and three-dimensional finite element software, the natural frequency and mode shape of linearized system are verified. With eigenvalue approximation, an analytical formula of the shaft bending resonant frequency is presented in this paper, and it can improve machine design and testing efficiency obviously.

Abbreviations

A_F: Exciting amplitude of shaker force
B: Horizontal distance from shaft end to wirerope end
$C_{1,2}$: Pendulum block centroid point
D: Vertical distance from pendulum block centroid to shaker force
F: Shaker exciting force
F_B: Shaft bending force load
F_N: Shaft axial normal load
g: Gravity acceleration
G: Vertical distance from pendulum block centroid to shaft axis
H: Vertical distance from pendulum block centroid to wirerope end
I: Rotational inertia of pendulum block
k: Suspending wirerope stiffness
K_F: Equivalent force bending stiffness of shaft
K_M: Equivalent moment bending stiffness of shaft
K_N: Equivalent axial normal stiffness of shaft
K_{NM}: Compound moment stiffness
L: Wirerope initial length
m: Pendulum block mass
m_0: Suspending roller mass
M_B: Shaft bending moment load
$P_{1,2}$: Wirerope end point
Q: Shaker force point
$Q_{1,2}$: Shaft end point
$s_{1,2}$: Suspending wirerope total elongation
t: Time
W: Half width of pendulum block
$x_{1,2}$: Horizontal displacement of pendulum block centroid
$X_{1,2}$: Horizontal displacement of suspending roller ring
$y_{1,2}$: Vertical displacement of pendulum block centroid
$z_{1,2}$: Wirerope vibrational elongation
$\alpha_{1,2}$: Swing angle of suspending wirerope
$\beta_{1,2}$: Swing angle of pendulum block
ω: Exciting frequency of shaker force
ω_n: Shaft bending resonant frequency.

Data Availability

The authors declare that all data can be available for readers and researchers to verify the results of this paper replicate the analysis and conduct secondary analyses.

Conflicts of Interest

The authors declare that they have no conflicts of interest or personal relationships that could have appeared to influence the work reported in this paper.

References

[1] M. Z. Mohammadi, S. Hassanifard, and A. Rahmatfam, "An evaluation of total fatigue life prediction of a notched shaft subjected to cyclic bending load," *Engineering Fracture Mechanics*, vol. 166, pp. 128–138, 2016.

[2] R. B. Carpinteri and A. Spagnoli, "Surface flaws in cylindrical shafts under rotary bending," *Fatigue and Fracture of Engineering Materials and Structures*, vol. 21, pp. 1027–1035, 1998.

[3] A. Schmid, M. Kluge, and E. Roos, "Fatigue strength under vibratory stresses and notch reduction of casehardened steel 25MoCr4 depending on various manufacturing processes for hollow transmission shafts," *Steel Research International*, vol. 82, no. 11, pp. 1278–1286, 2011.

[4] W. Y. C. Yu, K. S. Choi, J. Pan, and D. Close, "Testing and modeling of frequency drops in resonant bending fatigue tests

of notched crankshaft sections," *SAE Technical Paper*, vol. 01, p. 1501, 2004.

[5] J. I. Huertas, N. Navarrete, M. Giraldo, J. D. Uribe, and J. J. Gasca, "Resonant fatigue test bench for shaft testing," *Fatigue and Fracture of Engineering Materials and Structures*, vol. 40, no. 3, pp. 364–374, 2017.

[6] X. Z. Yu, Z. T. Liu, Y. M. Shen, and F. Qi, "An intelligent fatigue test system for crankshaft," *Acta Armamentarii*, vol. 25, pp. 368–371, 2004.

[7] X. L. Yu. Zhou and Xl Yu, "Fatigue crack growth rate test using a frequency sweep method," *Journal of Zhejiang University - Science*, vol. 9, no. 3, pp. 346–350, 2008.

[8] X. C. Lü, Z. Huang, and G. Q. Shu, "Modelling and experimental study on bending vibration of a diesel engine crankshaft," *Proceedings of the Institution of Mechanical Engineers - Part D: Journal of Automobile Engineering*, vol. 218, no. 4, pp. 385–394, 2004.

[9] L. Kasprzyczak and E. Macha, "Energy parameter control system of a polyharmonic bending and torsion testing machine," *Journal of Vibration and Control*, vol. 21, no. 13, pp. 2633–2638, 2015.

[10] K. Bao, R. D. Liao, and Z. X. Zuo, "Stress calculation of fillet rolled crankshaft in bending fatigue tests," *Applied Mechanics and Materials*, vol. 44-47, pp. 2798–2804, 2010.

[11] Y. L. Spiteri and R. Segar, *An exploration of failure modes in rolled, ductile, cast-Iron crankshafts using a resonant bending testing rig*, SAE Technical Paper, vol. 01, p. 1906, 2005.

[12] P. S. Patel, "Development of a computerized digital resonance fatigue test controller with load feedback management," *SAE Technical Paper*, vol. 01, p. 1620, 2006.

[13] M. Li Feng, "Development of a computerized electrodynamic resonant fatigue test machine and its applications to automotive components," *SAE Technical Paper*, vol. 01, p. 0951, 2003.